Colloids and Surfaces A: Physicochem. Eng. Aspects xxx (2013) xxx–xxx

Contents lists available at SciVerse ScienceDirect

Colloids and Surfaces A: Physicochemical and Engineering Aspects

journal homepage: www.elsevier.com/locate/colsurfa

Experimental and theoretical studies of scanning adsorption–desorption isotherms

Richard Cimino[a], Katie A. Cychosz[b], Matthias Thommes[b], Alexander V. Neimark[a,*]

[a] Rutgers University, Department of Chemical and Biochemical Engineering, 98 Brett Road, Piscataway, NJ 08854, USA
[b] Quantachrome Instruments, 1900 Corporate Dr., Boynton Beach, FL 33426, USA

HIGHLIGHTS

- Scanning isotherms provide important information about pore network geometry.
- A partial correlation model is suggested to distinguish pore blocking effects.
- A percolation model of scanning desorption isotherms is formulated.
- A computational method for calculating pore network connectivity and size distribution of pore necks is introduced.

GRAPHICAL ABSTRACT

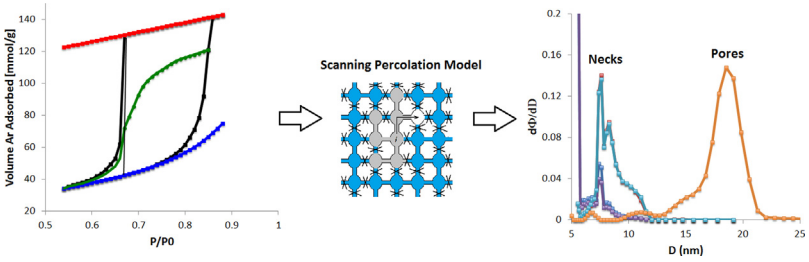

ARTICLE INFO

Article history:
Received 21 November 2012
Received in revised form 7 March 2013
Accepted 13 March 2013
Available online xxx

Keywords:
Mesoporous materials
Scanning
Hysteresis
Percolation

ABSTRACT

Scanning isotherms provide important information about the pore network geometry, including its connectivity and pore size distribution, which cannot be revealed from the main adsorption and desorption isotherms. We analyze scanning isotherms on different yet well-characterized pore structures: SBA-15 silica, KIT-6 silica, Vycor glass, and 3DOm carbons. Firstly, we suggest a partial correlation model to distinguish the importance of the pore blocking effects. Secondly, we formulate a percolation model for a quantitative description of scanning desorption isotherms in the pore and neck network in two versions, the analytical Bethe approximation and the Monte Carlo simulation on 3D cubic lattice. Thirdly, we introduce a computational method for calculating the pore network connectivity characterized by the network coordination number and the pore and neck size distributions.

1. Introduction

Capillary condensation hysteresis is one of the longest-studied and still enigmatic phenomena in adsorption science [1–4]. It is well documented, both experimentally and theoretically, that during the adsorption–desorption cycle, capillary condensation in mesopores (larger than ~4 nm in diameter) occurs generally at a higher pressure of adsorbing gas then evaporation. As such, adsorption and desorption isotherms form a pronounced hysteresis loop that is repeatable in subsequent cycles. A better understanding of the specifics of hysteretic behavior of adsorption and desorption isotherms is important for practical problems of pore structure characterization. The shape of the hysteresis loop contains information about the pore structure. The adsorption and desorption isotherms provide primary information about porosity, surface area, and pore size distribution, which are calculated from the experimental data using various empirical and theoretical methods [5,6].

Starting from the seminal work of Zsigmondy [7] published in 1913 and elaborated by Kraemer [8], McBain [9], Cohan [10,11], Schofield [12], de Boer [13], Dubinin [14] and Everett [1] among other prominent physicho-chemists, capillary condensation hysteresis has been studied based on the classical Kelvin-Laplace theory of capillarity using model cylindrical and ink-bottle pores.

* Corresponding author. Tel.: +1 732 445 0834.
E-mail address: aneimark@rutgers.edu (A.V. Neimark).

0927-7757/$ – see front matter © 2013 Elsevier B.V. All rights reserved.
http://dx.doi.org/10.1016/j.colsurfa.2013.03.025

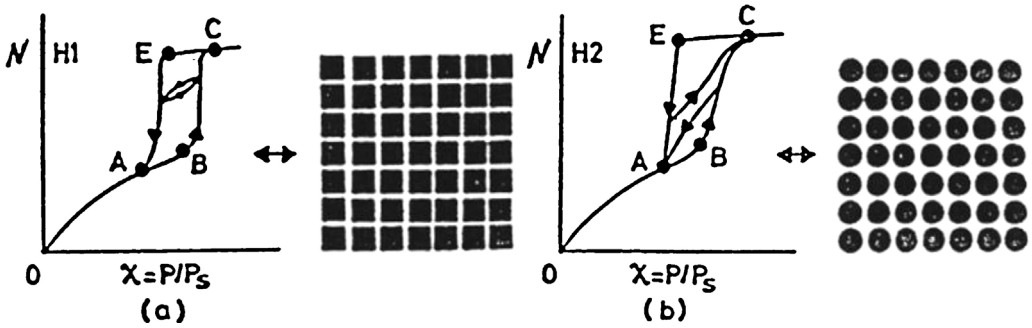

Fig. 1. Characteristic types of hysteresis behavior, H1 (left) and H2 (right). A and C are the lower and upper points of closure of the hysteresis loop; B and E correspond to the onsets of capillary condensation and evaporation, respectively.
Figure taken from Neimark [17].

The main hysteresis mechanisms were recognized: *delayed condensation* due to the formation of metastable adsorption films, *initiation of capillary condensation* upon condensation in neighboring smaller pores, *pore blocking* resulting in the delay of evaporation from the pores blocked by smaller ones, and *cavitation* in metastable condensed fluid at the tensile stress limit.

The theory of capillary hysteresis in individual pores culminated in the independent domain theory (IDT) developed by Everett and coauthors in the 1950s and discussed in detail in his seminal review [1]. This review can be considered as a watershed between the classical period of capillary hysteresis theory, which was based on the interfacial thermodynamics and simple geometrical models of pores, and the modern period of investigations related to the applications of methods of statistical physics of random networks and Monte Carlo simulations.

Arising from interplay of geometrical, topological, and thermodynamic factors, the characteristic features of capillary condensation hysteresis are quite distinct for different types of porous materials. Experimentally, these distinct features of adsorption hysteresis are prominently displayed in the behavior of scanning isotherms, which provide additional information about the pore network geometry, including its connectivity and pore size distribution that cannot be revealed from the main adsorption and desorption branches. Scanning isotherms are measured by reversing the direction of the gas pressure variation in the adsorption or desorption process. Scanning behavior has been studied extensively starting from the truly exceptional work of van Bemmelen published in 1897 [15] throughout the mid-20th century, furnishing an abundance of experimental data [1,16]. Theoretically, it has been well understood since the seminal works of Everett that the description of scanning isotherms cannot be achieved based on the models of adsorption in individual pores [1]; it is necessary to take into account a cooperative nature of capillary condensation and desorption processes in three dimensional pore networks with distributed geometrical parameters of individual pores.

Two characteristic types of hysteresis behavior are distinguished in hysteresis loops of type H1 and H2 by IUPAC classification [5] (Fig. 1). In materials with pore networks formed by channels with unimodal pore size distributions, the scanning isotherms form closed loops crossing the main hysteresis loop of type H1. This behavior is observed in ordered structures like MCM-41, SBA-15, and controlled porous glasses (CPG). In materials consisting of pore channels with alternating enlargements (voids) and constrictions (necks), the scanning isotherms approach the upper and lower points of closure of the main hysteresis loop of type H2. This behavior is observed in disordered structures like Vycor and silica gel. The IUPAC classification reflects ideal structures, yet it is useful for revealing the main mechanisms of capillary phenomena in pore networks.

Application of the percolation theory to capillary condensation hysteresis in pore networks originates from the pioneering works of Wall and Brown [18] Neimark [19–21] and Mason [22,23]. Wall and Brown [18] performed Monte Carlo simulations to account for the pore blocking effects during desorption. Neimark et al. [19,21] considered the pore blocking effects during desorption, as well as for initiated capillary condensation during adsorption, in pore networks with an uncorrelated distribution of pore sizes using the bond percolation model in the Bethe approximation. The Bethe network model of pores connected by necks was employed by Mason [22,23] and Neimark [24] to describe the capillary hysteresis of Xe on Vycor glass to improve the independent domain theory model of Everett [1]. Neimark [24] and later Mason [25] and Parlar and Yortsos [26] suggested very similar theories of scanning adsorption and desorption isotherms utilizing the Bethe network model with different coordination numbers. The cavitation mechanism of desorption was incorporated in the percolation model by Parlar and Yortsos [27].

Wilkinson and Willemsen [28] introduced the model of invasion percolation to describe the propagation of the interface between wetting and non-wetting phases into the pore network in the processes of wetting. However, the invasion percolation model does not account for the volatility of wetting liquid and is not directly applicable to vapor adsorption. It should be noted that starting from the initial papers [18,21] it was understood the percolation model offers a unified description of the desorption of condensed wetting fluid and the intrusion of non-wetting fluid. The percolation theory of scanning mercury intrusion–extrusion cycles was developed by Neimark [29,30].

Modeling of adsorption and desorption processes in three-dimensional (3D) pore networks was performed in many further works by using various computational algorithms [31–35]. One of the most advanced is the dual pore-site network model suggested by Mayagoitia et al. [36]. This model implies direct simulation of the capillary condensation and desorption processes in 3D networks with randomly distributed pore and neck sizes, which determine the conditions of pore filling and emptying. Within the dual pore-site model, Cordero et al. [37] and Rojas et al. [38] simulated both scanning adsorption and desorption isotherms for various 3D networks. Although the primary goal of the percolation models was the development of improved methods for pore size analysis [31,32,39], there were no successful attempts to incorporate into the characterization methods the information contained in the scanning isotherms.

The main aim of this paper is to lay groundwork for developing a practical methodology for calculating the network connectivity and pore size distributions from the scanning isotherms. This aim is especially topical now due to the recent advances in high-precision automated measurements of scanning isotherms [40]

Please cite this article in press as: R. Cimino, et al., Experimental and theoretical studies of scanning adsorption–desorption isotherms, Colloids Surf. A: Physicochem. Eng. Aspects (2013), http://dx.doi.org/10.1016/j.colsurfa.2013.03.025

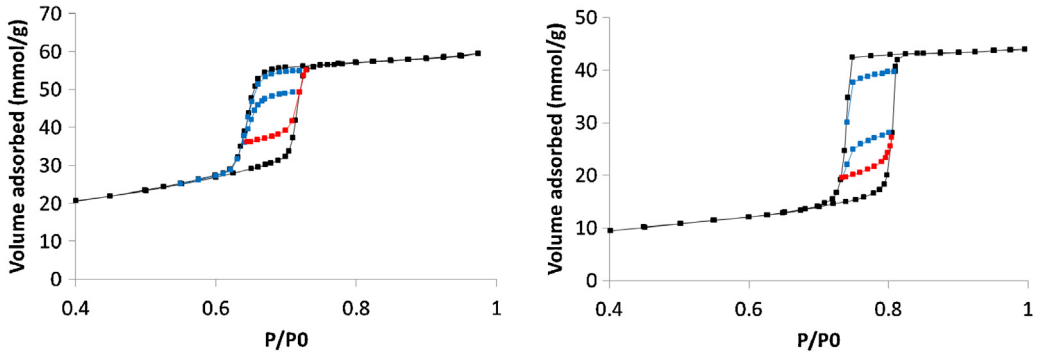

Fig. 2. Nitrogen (77 K) primary (black) and scanning adsorption (red) and desorption (blue) isotherms on SBA-15 (left) and KIT-6 (right) samples. Note the closed loop structure, associated with H1 type materials. (For interpretation of the references to color in this sentence, the reader is referred to the web version of the article.)

and the necessity to characterize the pore structure of novel designer porous materials, the list of which has been increasing exponentially during last two decades [2,41–43]. In Section 2, we present a series of scanning isotherms measured on selected samples of SBA-15 silica, KIT-6 silica, and 3DOm carbon materials. The SBA-15 example and the literature data on Xe adsorption on Vycor [1] represent case-study systems for evaluation of the limits of applicability of the independent pore models, which are discussed in Section 3. After analysis of the conventional deterministic and uncorrelated models, we suggest a partial correlation model (PCM) and show that this model provides a quantitative test for networking effects. We show that while PCM provides a reasonable quantitative description of scanning adsorption isotherms for all systems considered the deviation between theoretical and experimental scanning desorption isotherms points toward the importance of accounting for the pore blocking effects in 3D networks of Vycor, KIT-6, and 3DOm structures. The percolation models of scanning hysteresis loops are discussed in Section 4. Here, we first elaborate on the earlier work of Neimark [24] and formulate the theory of scanning isotherms using the Bethe approximation. Then, we perform direct modeling of scanning desorption isotherms using Monte Carlo simulation on the 3D cubic lattice. We compare the theoretical and experimental results for selected systems. Section 5 is devoted to the formulation of the practical methodology for calculating the *network connectivity* defined as an effective coordination number linked to the percolation threshold and the *neck size distribution* from the main and scanning desorption isotherms. Thus, the determined neck size distribution complements the pore size distribution calculated from the main adsorption isotherm. This methodology is verified on Vycor and applied to 3DOm samples. The main conclusions are summarized in Section 6, where we justify and suggest the proposed methodology for advanced characterization of mesoporous materials.

2. Experimental studies

2.1. SBA-15 and KIT-6 silicas

As typical examples of H1 hysteresis behavior, we have chosen SBA-15 and KIT-6 silicas. SBA-15 is a silica material with a hexagonally ordered 2D array (*p6m* symmetry) of cylindrical channels [44]. SBA-15 samples are often used for reference measurements due to their simple pore geometry in order to validate the theoretical models [45,46]. It is commonly assumed that adsorption and desorption processes occur in the SBA-15 channels independently providing a case-study system for the IDT model (see Fig. S1 in Supplementary Information for DFT pore analysis of SBA-15). The pore network in KIT-6 silica represents 3D gyroidal structure of cubic (*Ia3d*) symmetry [47,48] exhibiting network effects [49]. Adsorption–desorption isotherms on both samples, Fig. 2, form a prominent H1 hysteresis loop. Scanning isotherms cross the main hysteresis loop as expected in the schematics of Fig. 1(left).

2.2. 3DOm carbon

Recently discovered 3D ordered mesoporous carbons (3DOm) are obtained by hard templating of silica spherical nanoparticle colloidal crystals [50]. The pore network geometry in 3DOm carbons is composed of spherical voids, or cages formed in place of silica nanoparticles, which are connected by narrow windows, or necks. Four samples produced from nanoparticles of different size, 10, 20, 30, and 40 nm, were studied. For the cage-like pore network geometry, one would expect to get an H2 hysteresis loop, as in Fig. 1(right). However, as shown in Fig. 3, the adsorption–desorption isotherms presented are of H1 type, and the behavior of scanning isotherms, especially for samples with smaller pores, is similar to that on SBA-15 and KIT-6. As the pore size progresses up to 40 nm, the hysteretic behavior becomes more complex and reflects the existence of some secondary pore structure. Also, it was shown that the isotherms on the 40 nm sample are affected by a secondary pore structure displayed by a prominent inflexion of the main adsorption branch at $P/P_0 \sim 0.85$ (Fig. 3 bottom right). In our earlier work [40], 3DOm carbons were analyzed by N2 and Ar gas adsorption, and it has been suggested that the pore blocking mechanism plays an important role in the desorption process.

2.3. Vycor glass

Vycor glass is siliceous compound, which is formed by the thermal spinodal decomposition of a two-phase alkali-borosilicate–silica solution upon cooling. During the decomposition, the phases separate and the borosilicate is dissolved away, leaving a highly disordered silica matrix that possesses a network of pores with alternating enlargements and constrictions [51]. Detailed simulation of the pore structure formation during spinodal decomposition was performed using molecular simulations by Gelb and Gubbins [52]. Vycor glass has been playing an extremely important role in the theory of adsorption as a case-study example of disordered pore networks due to availability of high-resolution experimental data and a consensus among the researchers about the specifics of its pore system geometry. The experimental data on xenon (151 K) adsorption and desorption scanning on Vycor collected by Brown in 1963 and presented in the review of Everett [1,16], served as a benchmark for many theories of capillary condensation, starting from the IDT of Everett to percolation models of Mason [23,25] Neimark [20,24], Parlar and Yortsos [26] and Seaton et al. [32] to lattice DFT models of Monson, Kierlik, and Rosinberg [53], among the others. This data re-plotted in Fig. 4 represents a

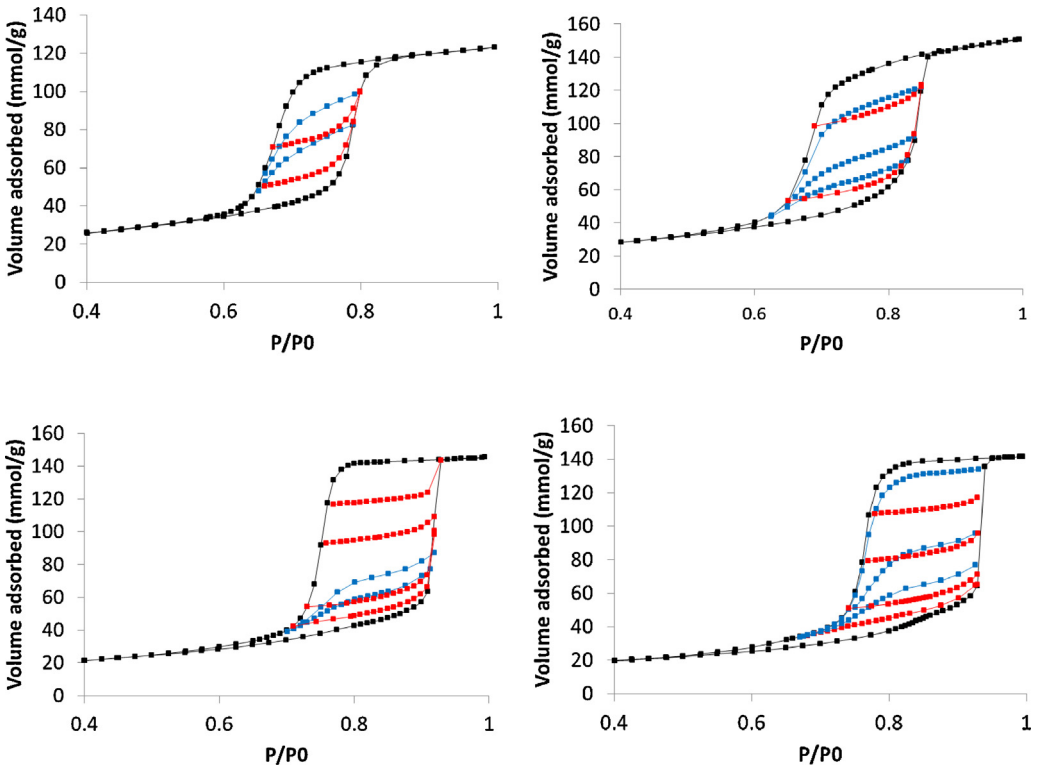

Fig. 3. Argon (87 K) primary (black) and scanning adsorption (red) and desorption (blue) isotherms on four 3DOm carbons templated on colloidal crystals of 10, 20, 30 and 40 nm silica nanoparticles (top left to bottom right). Note the following characteristic features: the boundary hysteresis loop for all samples is of type H1; while the scanning isotherms on the10 nm sample are qualitatively similar to those on SBA-15 and KIT-6 (Fig. 2), as the pore size increases the desorption scanning isotherms tend to bend; the isotherms on the 40 nm sample are affected by a secondary pore structure displayed by a prominent inflexion of the main adsorption branch at P/P_0 ~0.85. (For interpretation of the references to color in this sentence, the reader is referred to the web version of the article.)

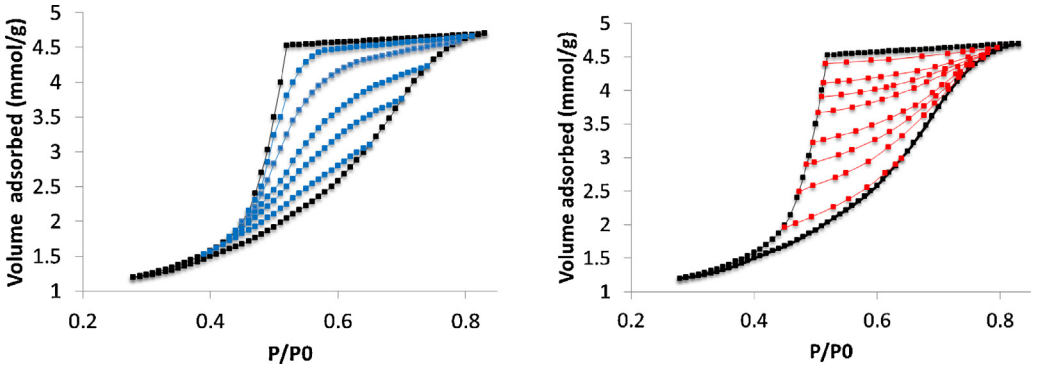

Fig. 4. Xenon (151 K) adsorption (left) and desorption (right) scanning isotherms on Vycor glass. Note typical H2 type hysteresis behavior; the scanning isotherms converge at the closure points of the hysteresis loop.
Data reprinted and units converted from Everett [1].

typical H2 hysteresis behavior in compliance with the schematic of Fig. 1(right). The main hysteresis loop has a prominent triangular shape. The scanning isotherms converge at the closure points of the hysteresis loop rather that crossing the loop as in the case of H1 hysteresis.

The hysteresis behavior shown in Fig. 4 for xenon adsorption is typical for other adsorbates on Vycor. In Fig. 5, experimental data for N2 (77 K) adsorption is presented that have the same features.

3. Models of independent pores

The IDT model of adsorption proposed by Everett [1,54,55] is based on an assumption that the pore space may be subdivided into individual regions or 'domains', which are non-interacting and adsorb and desorb independently of one another. The assumption of pore independence is explicitly or implicitly used in all conventional methods of pore structure characterization from BJH to DFT methods, which ignore the cooperative mechanisms of capillary condensation and desorption due to pore networking effects. At the same time, DFT based independent pore models can correctly determine the underlying mechanism of condensation, i.e. the existence of metastable pore fluid associated with condensation, and when applicable, provide the most straightforward methods for practical applications.

Following Everett [1], each pore treated as an independent domain is characterized by two parameters, the relative pressures of condensation χ_+ and desorption χ_-. These pressures depend on the pore size and shape. Standard methods of calculating pore size distributions often assume that pores are cylindrical and the pore diameter d_p determines the pressures of condensation and

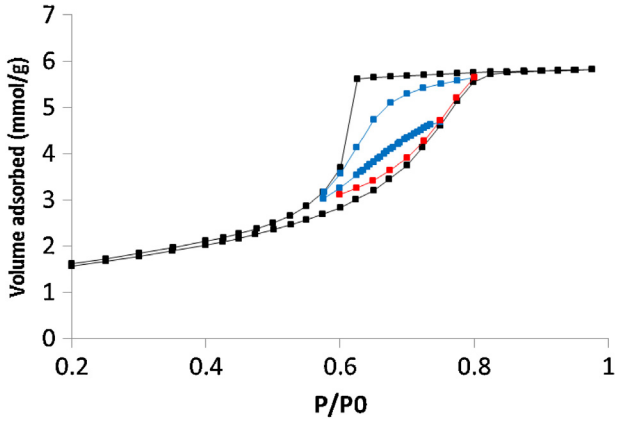

Fig. 5. N2 (77 K) primary (black) and scanning adsorption (red) and desorption (blue) isotherms on Vycor glass. Note the typical scanning behavior for H2 type hysteresis similar to that of xenon shown in Fig. 4. (For interpretation of the references to color in this sentence, the reader is referred to the web version of the article.)

desorption, $\chi_+(d_p)$ and $\chi_-(d_p)$. As such, there exists a one-to-one correspondence between adsorption and desorption pressures for a particular pore: for every relative pressure point $\chi_a = \chi_+(d_p)$ along the adsorption boundary curve there exists a companion point on the desorption boundary curve, $\chi_d = \chi_-(d_p)$. We will call a model, which is based on this assumption, a *deterministic model*. The alternative approach within the independent pore models, which also dates back to Everett [1] and was accepted in earlier works on percolation models [17,18,22–25,39], is to assume that the pressures of condensation χ_+ and desorption χ_- in a given pore are not correlated: the former is determined by the pore size d_p as $\chi_+(d_p)$ and the latter is determined by the neck size d_n as $\chi_-(d_n)$. In case of multiple necks, d_n represents the size of the largest neck. This assumption is equivalent to the assumption of the absence of correlation between the pore and neck sizes, and is called an *uncorrelated model*.

Below, we propose a *partial correlation model* within the independent domain theory, as a compromise between the deterministic and uncorrelated models, and suggest a method for assessing the significance of networking effects. However, first, we have to introduce a method how to convert the experimentally measured adsorption isotherms, which represent the adsorbed amount measured in experiments, into the fractions of filled and unfilled pores, which are required for modeling the adsorption process in a network of pores.

3.1. Reference isotherms and fractions of filled and unfilled pores.

In the process of gas adsorption, an individual pore may exist in two states, *unfilled*, when the pore walls are covered by adsorption films and the pore center is occupied by vapor-like adsorbate, and *filled*, when the whole pore volume is occupied by liquid-like, condensed adsorbate. The transitions between these states are associated with the capillary condensation and capillary evaporation (desorption) transitions. Consequently, one calls the adsorbate state in unfilled pores as vapor-like, the adsorbate state in filled pores as liquid-like. In order to relate the processes of pore filling and emptying to measured adsorption and desorption isotherms, it is necessary to separate the adsorption in unfilled and filled pores. To this end, we introduce the reference isotherms in unfilled and filled pores, $V_s(\chi)$ and $V_c(\chi)$. The former represents an interpolation of the reversible adsorption isotherm to the hysteresis region and reflects the build-up of the adsorption film. The film isotherm $V_s(\chi)$ is modeled as

$$V_s(\chi) = S \cdot h(\chi) \tag{1}$$

where S is the surface area of the adsorbent and $h(\chi)$ is the effective thickness of the adsorbed layer that is proportional to the reference adsorption isotherm on a non-porous surface of the same origin. Eq. (1) is a standard approximation that does not take into account the pore wall curvature. The film reference isotherm is commonly modeled with the FHH equation with specific adsorbent–adsorbate parameters K and m:

$$h(\chi) = \left(\frac{K}{-\ln \chi}\right)^{1/m} \tag{2}$$

Parameters K and m are chosen such that the effective thickness is in Ångstroms. Below, we employ the recommended parameters used for validation of the NLDFT models [56]: for nitrogen–silica adsorption, $K = 44.54$ and $m = 2.241$; for argon–silica adsorption, $K = 73.17$ and $m = 2.665$. The specific surface area, S, can be determined in several ways. In the examples considered below, S was found by aligning the boundary adsorption isotherm with the reference isotherm, using S as a fitting parameter. The BET surface area may serve as a starting point for such fitting. We found that in general, the BET and fitted surface areas differed by 15% or less for all sample materials. (See Supplementary Information for details)

The reference desorption isotherm $V_c(\chi)$ reflects compressibility of condensed fluid in filled pores and related effects. $V_c(\chi)$ should be determined by extrapolation of the reversible part (upper plateau) of the desorption isotherm starting from the upper closure point C of the main hysteresis loop. In the first approximation, it can be modeled by a tangent to the desorption isotherm at the capillary condensation pressure, χ_c, as

$$V_c(\chi) = \left(\frac{dV}{d\chi}\right)|_{\chi c}(\chi - \chi_c) + V(\chi_C) \tag{3}$$

Using the reference isotherms $V_s(\chi)$ and $V_c(\chi)$, the experimental isotherm $V(\chi)$ may be presented through the fraction of unfilled pores at the relative pressure χ, $Q(\chi)$, as

$$V(\chi) = V_s(\chi) \cdot Q(\chi) + (1 - Q(\chi)) \cdot V_c(\chi) \tag{4}$$

From this equation, the fraction of unfilled pores $Q(\chi)$ is estimated in the region of hysteresis as

$$Q(\chi) = \frac{V_c(\chi) - V(\chi)}{V_c(\chi) - V_s(\chi)} \tag{5}$$

Beyond the hysteresis region, $Q(\chi) = 0, \quad \chi < \chi_A; \quad 1, \quad \chi > \chi_C$

The fractions of unfilled pores on the main adsorption or desorption isotherms are determined from Eq. (5), as

$$Q_+(\chi) = \frac{V_c(\chi) - V_+(\chi)}{V_c(\chi) - V_s(\chi)}, \qquad Q_-(\chi) = \frac{V_c(\chi) - V_-(\chi)}{V_c(\chi) - V_s(\chi)} \tag{6}$$

The transition from the hysteresis loop formed by the experimental adsorption–desorption isotherms to the hysteresis loop formed by the fractions of unfilled pores is illustrated in Fig. 6 with the example of the SBA-15 isotherm given in Fig. 2(left). The positions of points A, B, C, and E were determined by expert choice with accuracy of ~2% (see Supplementary Information for details).

Eq. (4) is applicable for any isotherm. For the scanning adsorption $V_+(\chi, \chi_d)$ and desorption isotherms $V_-(\chi, \chi_a)$ it reads:

$$V_+(\chi, \chi_d) = V_s(\chi) \cdot Q_+(\chi, \chi_d) + (1 - Q_+(\chi, \chi_d)) \cdot V_c(\chi) \tag{7}$$

$$V_-(\chi, \chi_a) = V_s(\chi) \cdot Q_-(\chi, \chi_a) + (1 - Q_-(\chi, \chi_a)) \cdot V_c(\chi) \tag{8}$$

Here and below, we use the denotations $(\chi, \chi_{a/d})$ to define the scanning isotherms that originate from points $\chi_{a/d}$ on main adsorption or desorption isotherms.

The uncorrelated model implies that the fraction of unfilled pores during scanning adsorption, $Q_+(\chi, \chi_d)$, decreases from its initial value $Q_-(\chi_d)$, as

$$Q_+(\chi, \chi_d) = Q_-(\chi_d) \cdot (1 - Q_+(\chi)) \tag{9}$$

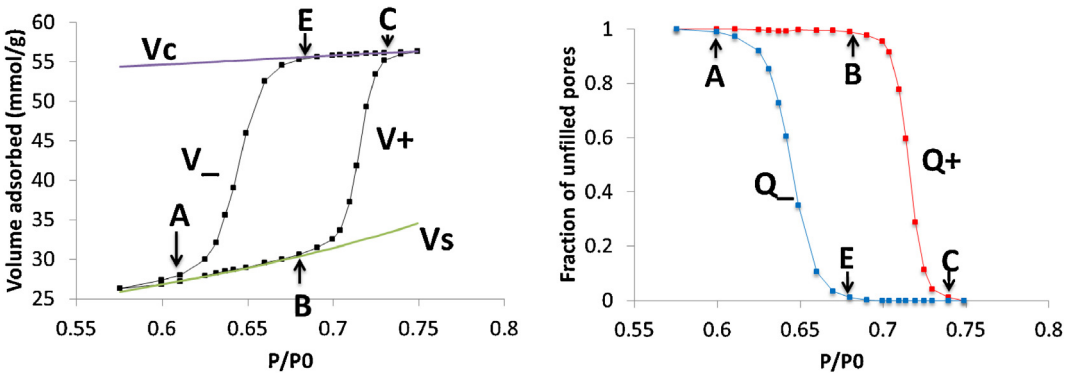

Fig. 6. Left – main hysteresis loop for the nitrogen adsorption–desorption cycle on SBA-15. Right – The main hysteresis loop recalculated via Eq. (6) in terms of the fractions of unfilled pores along the adsorption and desorption isotherms, Q_+ and Q_-.

This equation states that the probability of a pore that was unfilled at $\chi = \chi_d$ to be filled at the current relative pressure χ is equal to the fraction of filled pores, $1 - Q_+(\chi)$, on the main adsorption isotherm at χ. Similarly, the fraction of unfilled pores during scanning desorption, $Q_-(\chi, \chi_a)$, increases from its initial value $Q_+(\chi_a)$ as the pressure decreases, as

$$Q_-(\chi, \chi_a) = Q_+(\chi_a) + (1 - Q_+(\chi_a))\, Q_-(\chi) \tag{10}$$

This equation states that the probability of a pore that was filled at $\chi = \chi_a$ to be unfilled at the current relative pressure χ is equal to the fraction of unfilled pores, $Q_-(\chi)$ on the main desorption isotherm at χ. The scanning isotherms are determined by Eq. (8) with the fractions of unfilled pores calculated with Eqs. (9) and (10). The theoretical scanning isotherms in the uncorrelated model implies that the scanning isotherms approach the closure points of the main hysteresis loop, as for the H2 type hysteresis in Fig. 1 (right). It was shown [20,24] that the *uncorrelated model* describes with Eqs. (7)–(9) almost quantitatively the scanning adsorption isotherms on Vycor glass, but it fails to predict the shape of scanning desorption isotherms shown in Fig. 4. This inconsistency was interpreted by the importance of pore blocking percolation effects, which make desorption a cooperative process in a sense that the evaporation events in different pores occur in a correlated manner.

3.2. Partial correlation model

The uncorrelated model implies that the scanning isotherms converge at the points of closure of the main hysteresis loop. In order to extend the independent pore model to more general situations, when the scanning adsorption–desorption isotherms form close loops intersecting the main hysteresis loop, we introduce a partial correlation model (PCM). PCM is based on experimental observation that in the absence of networking effects the shape of the scanning isotherm resembles the shape of the main isotherm. As such, PCM implies that the fraction of unfilled pores $Q_-(\chi, \chi_a)$ along the scanning desorption isotherm is a linear function of the fraction of unfilled pores $Q_-(\chi)$ along the main desorption isotherm. For scanning desorption starting at $\chi = \chi_a$ and approaching the boundary desorption branch at $\chi = \chi_d$,

$$Q_-(\chi, \chi_a) = Q_+(\chi_a) + (Q_-(\chi_d) - Q_+(\chi_a)) \left(\frac{Q_-(\chi)}{Q_-(\chi_d)} \right) \tag{11}$$

Similarly, the fraction of unfilled pores $Q_+(\chi, \chi_d)$ along the scanning adsorption isotherm is assumed to be a linear function of the fraction of unfilled pores $Q_+(\chi)$ along the main adsorption isotherm. For scanning adsorption starting at $\chi = \chi_d$ and approaching the boundary adsorption branch at $\chi = \chi_a$,

$$Q_+(\chi, \chi_d) = Q_-(\chi_d) - (Q_-(\chi_d) - Q_+(\chi_a)) \left(\frac{1 - Q_+(\chi)}{1 - Q_+(\chi_a)} \right) \tag{12}$$

Note that Eq. (11) is reduced to Eq. (9) of the uncorrelated model at $\chi_d \to \chi_A$ and, respectively, Eq. (12) is reduced to Eq. (10) of the uncorrelated model at $\chi_a \to \chi_C$.

As shown in Fig. 7, the PCM, Eqs. (11) and (12), is in reasonable agreement with experimental scanning isotherms, both adsorption and desorption, on SBA-15 and KIT-6 samples with the characteristic H1 hysteresis loops. In the case of H2 hysteresis, PCM predictions agree with the scanning adsorption data and strongly deviate from the scanning desorption (Fig. 10). Deviations from the predictions of the independent pore model points toward the importance of the networking effects, which are more pronounced during desorption due to the pore blocking effect. In this way, PCM serves as a test of the pore blocking effects, which in particular are pronounced in disordered pore networks like that of Vycor glass during desorption.

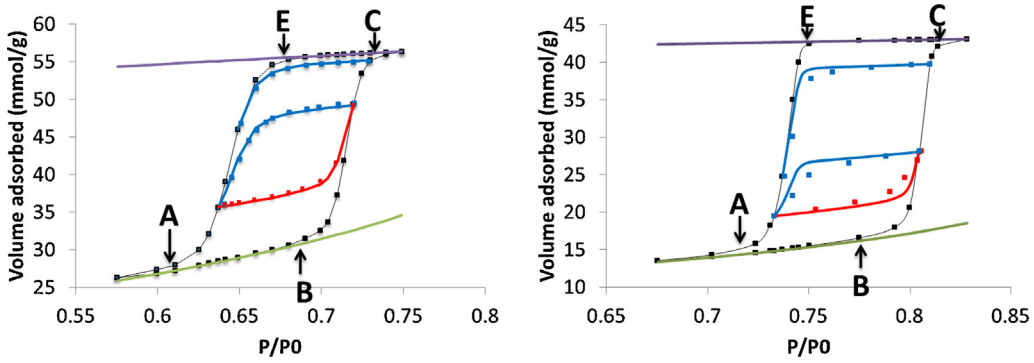

Fig. 7. Comparison of PCM with experiments for N_2 adsorption on SBA-15 (left) and KIT-6 (right).

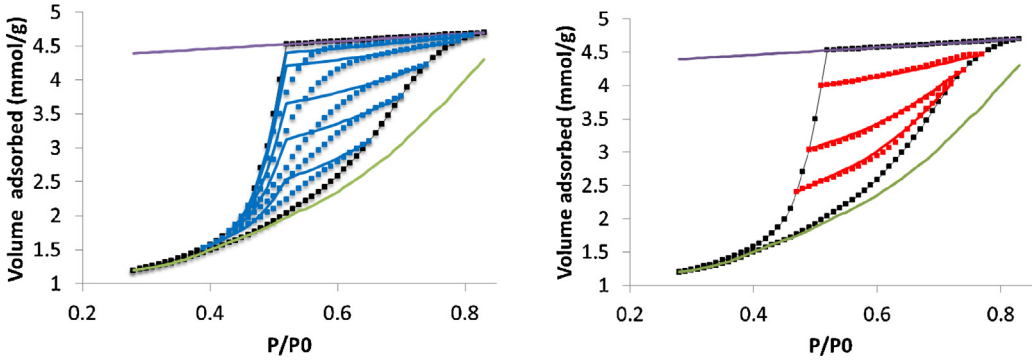

Fig. 8. Comparison of the PCM with experiments for Xe adsorption on Vycor glass; scanning desorption left, scanning adsorption (right). Experimental data taken from Everett [1].

PCM has the following interpretation in the ink-bottle pore model. Indeed, within the assumption of independent pores, the pressure of condensation χ_+ in a given pore is determined by the size d_p of the pore and the pressure of desorption χ_- is determined by the size d_n of the largest neck. Let us suppose that larger pores have a higher probability to have larger necks, particularly, that the pores larger than d_p have at least one neck larger than $d_n = g(d_p)$, where g is a certain monotonic function. In this case, the scanning desorption isotherm, $V_-(\chi, \chi_a)$, that originates at $\chi = \chi_a = \chi_+(d_p)$ must merge with the main desorption isotherm at $\chi = \chi_d = \chi_-(d_n)$. Indeed, the fraction $Q_+(\chi_a(d_p))$ of unfilled pores in the beginning of scanning desorption at $\chi_a = \chi_+(d_p)$ represents the fraction of pores larger that d_p and these pores have necks larger than d_n. Along the main desorption isotherm at $\chi = \chi_d = \chi_-(d_n)$, the fraction of unfilled pores $Q_-(\chi_d(d_n))$ includes the fraction of pores larger than d_p, $Q_+(\chi_a(d_p))$, plus the fraction of pores that are smaller than d_p but have necks larger than d_n. The fraction of this latter group of pores equals $Q_-(\chi_d) - Q_+(\chi_a)$. These are the pores, from which the condensed adsorbate evaporates along the scanning desorption path $V_-(\chi, \chi_a)$ initiated at $\chi_a = \chi_+(d_p)$, so that the scanning and the main desorption isotherms should meet at $\chi = \chi_d = \chi_-(d_n)$, and $V_-(\chi, \chi_a)\big|_{\chi=\chi_d=\chi_-(d_n)} = V_-(\chi)\big|_{\chi=\chi_d=\chi_-(d_n)}$. Respectively, the scanning adsorption isotherm that originates at $\chi_d = \chi_-(d_n)$ should merge with the boundary adsorption isotherm at $\chi_a = \chi_+(d_p)$, forming a closed scanning hysteresis loop.

4. Percolation models

The networking effects are most prominently displayed during the desorption process, which occurs in a cooperative fashion as the condition of evaporation from a given pore depends on the neighboring pores. When the pore is not blocked and condensed fluid has an interface with the vapor phase, evaporation occurs at the equilibrium relative pressure χ_e which is determined by the pore size. If the pore is blocked by narrower pores, the condensed fluid cannot evaporate at $\chi = \chi_e$ and becomes metastable at $\chi < \chi_e$. These pores we call metastable at given χ. Evaporation may occur only when the pore is connected to the vapor phase by a series of metastable pores. Only when this condition is met, the vapor–liquid interface, or meniscus, may percolate through the network and initiate evaporation of the metastable fluid at a relative pressure that is smaller than the equilibrium one. This mechanism is called in the literature the pore-blocking or percolation mechanism.

When the size of blocking pores is so small that the condensed fluid approaches the limit of metastability and evaporates spontaneously even though the neighboring pores are still filled, one deals with the cavitation mechanism. Cavitation, as was recently shown [57,58], takes places in the range of relative pressures 0.50–0.42 for nitrogen adsorption at 77.4 K and it is characterized by the abrupt step on the desorption isotherm. In the following percolation model, we do not consider the cavitation mechanism, since it is not relevant for the systems studied in this work.

4.1. Desorption from a pore network as a percolation process

Let us consider the desorption process in a network comprised of pores connected by narrower necks, Fig. 1 (right). In this model, the pores represent the network sites and the necks represent the network bonds. The following discussion is based upon the ideas put forward in the earlier works of one of us [20,24]. We assume that desorption is controlled by the size of necks, and the condensed fluid is "ready" to evaporate from any pore at given relative pressure χ provided that the condition of the vapor–liquid interface formation is met. This condition along the scanning desorption isotherm $V_-(\chi, \chi_a)$ is met in two cases schematically illustrated in Fig. 9. The pore must be connected by a continuous chain of metastable necks either with the external surface of the sample, or with an initially unfilled pore, in which the interface existed in the beginning of desorption at $\chi = \chi_a$. In other words, in order to trigger desorption, the meniscus must percolate to the pore either from the external surface, or from an initially unfilled pore.

To account for this condition, we introduce a probability factor $\alpha(q(\chi), Q_+(\chi_a))$ which depends upon the fraction of metastable necks $q(\chi)$ and the fraction of unfilled pores in the beginning of scanning, $Q_+(\chi_a)$. This factor is interpreted as the probability of finding a path of metastable necks by which a randomly chosen pore is connected to the vapor–liquid interface. As such, the fraction of unfilled pores along the scanning isotherm is the sum of the fraction of initially unfilled pores and the fraction of initially filled

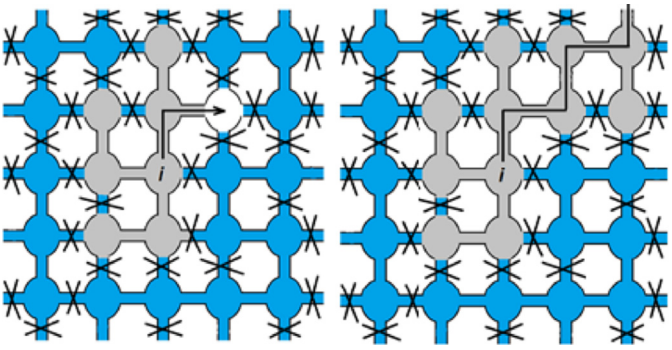

Fig. 9. Two pathways for evaporation: pore i is connected with the external surface by metastable necks (left) and pore i is connected with an initially unfilled pore (colored white) by metastable necks. Stable necks are crossed, filled pores are blue, unfilled pores are gray. (For interpretation of the references to color in this sentence, the reader is referred to the web version of the article.)

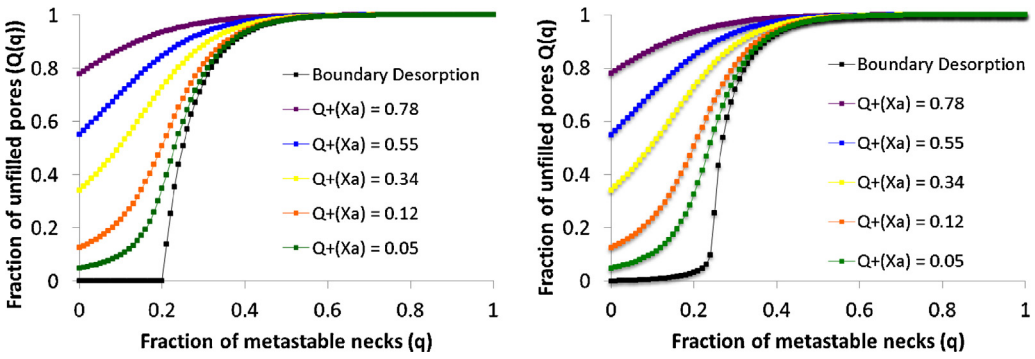

Fig. 10. The fraction $Q_{-}(q, Q_{+})$ of unfilled pores (right) along the main ($Q_{+} = 0$) and scanning desorption isotherms; values of $Q_{+} = 0.05, 0.12, 0.34, 0.55, 0.78$ correspond to the desorption isotherms of Xe on Vycor glass shown in Fig. 4(left). Coordination number $z = 6$. Bethe approximation (left), percolation threshold $q_c = 0.2$. MC simulation on the cubic lattice of $200 \times 200 \times 200$ sites (right) percolation threshold $q_c \approx 0.25$. The rounding of the percolation probability at the threshold is caused by the boundary effects.

pores multiplied by the probability of the existence of a metastable pathway:

$$Q_{-}(\chi, \chi_a) = Q_{+}(\chi_a) + (1 - Q_{+}(\chi_a)) \cdot \alpha(q(\chi), Q_{+}(\chi_a)) \quad (13)$$

For the main desorption branch ($Q_{+} = 0$), meniscus percolation originates from the external surface only, and the probability of desorption $\alpha(q, 0)$ reduces to the percolation probability $Q_p(q)$ in the classical bond percolation problem [20], $\alpha(q, 0) = Q_p(q)$, and

$$Q_{-}(\chi) = Q_p(q(\chi)) \quad (14)$$

The percolation probability for a macroscopically large network is a step-wise function. Below the percolation threshold q_c, $Q_p(q) = 0$ at $q < q_c$. This means that until the fraction of metastable pores is below the percolation threshold, evaporation may occur only from the pores located near the external surface of porous body, since the probability that a pore in the bulk of the sample is connected with the external surface by a chain of metastable necks is zero. The percolation probability rapidly increases above the percolation threshold, as $Q_p(q) \propto (q - q_c)^{\beta}$. For 3D networks, $\beta \approx 0.46$ [59]. As such, in the framework of the percolation theory, the onset of desorption from a fully saturated network indicated as point E in Figs. 1–10 corresponds to the percolation threshold,

$$q(\chi_E) = q_c. \quad (15)$$

The process of evaporation of condensed fluid along the scanning desorption isotherm begins at $\chi > \chi_E$ provided that $q(\chi) > 0$. The probability factor $\alpha(q, Q_{+})$ monotonically increases with q at given $Q_{+} > 0$. A general analytical expression for $\alpha(q, Q_{+})$ for three-dimensional networks does not exist. It depends on the pore connectivity, or the network coordination number z, and also on the network topology. Below, we use two approaches to determine $\alpha(q, Q_{+})$.

4.1.1. Bethe approximation

The Bethe approximation was employed in early works on percolation models of capillary phenomena [19–23] and it was shown to provide a qualitatively correct description of the percolation process. The Bethe approximation neglects the topological correlations of the distribution of network elements caused by the existence of cycles in real networks that makes possible an analytical solution. The percolation probability $Q_p(q)$ in the Bethe network with the coordination number z is defined from the following system of algebraic equations,

$$Q_p(q) = 1 - y^z, \qquad y = (1 - q) + qy^{z-1} \quad (16)$$

where y is the probability that the desired path through the metastable necks does not exist provided that the first step is taken toward one of z neighboring sites. The percolation probability $Q_p(q)$ vanishes below the percolation threshold

$$q_c = \frac{1}{z - 1} \quad (17)$$

The problem of desorption from a partially saturated pore network is a bond-site percolation problem [24] since the probability α of desorption from an initially filled site depends on both the fraction q of the metastable bonds and the fraction Q_{+} of the initially unfilled sites. The probability factor $\alpha(q, Q_{+})$ fulfills the system of algebraic equations, similar to (16),

$$\alpha(q, Q_{+}) = 1 - y^z, \qquad y = (1 - q) + q(1 - Q_{+}) \cdot y^{z-1} \quad (18)$$

Eq. (18) considers that the probability y is equal to the sum of probabilities of the following events: (1) the chosen neck is stable (probability $1 - q$) and (2) the chosen neck is metastable (probability q) and leads to an initially filled site (probability $1 - Q_{+}$) but all $z - 1$ paths from this site fail to connect it with an initially unfilled site (probability y^{z-1}). The function $\alpha(q, Q_{+})$ for the Bethe network with the coordination number $z = 6$ is presented in Fig. 12 together with the respective fraction $Q_{-}(q, Q_{+})$ of unfilled pores along the primary and scanning desorption isotherms determined by Eq. (13).

4.1.2. 3D lattice simulation

The bond-site percolation process can be directly simulated on a 3D network to determine the fraction of unfilled pores $Q_{-}(q, Q_{+})$ along primary and scanning desorption curves as a function of the

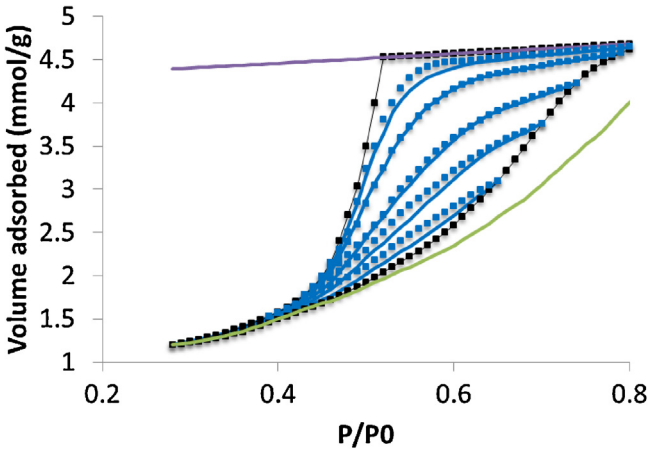

Fig. 11. Experimental and predicted scanning isotherms for Xe adsorption on Vycor glass, using the Bethe approximation and fitted the coordination number $z = 6.6$. Experimental data from Everett [1].

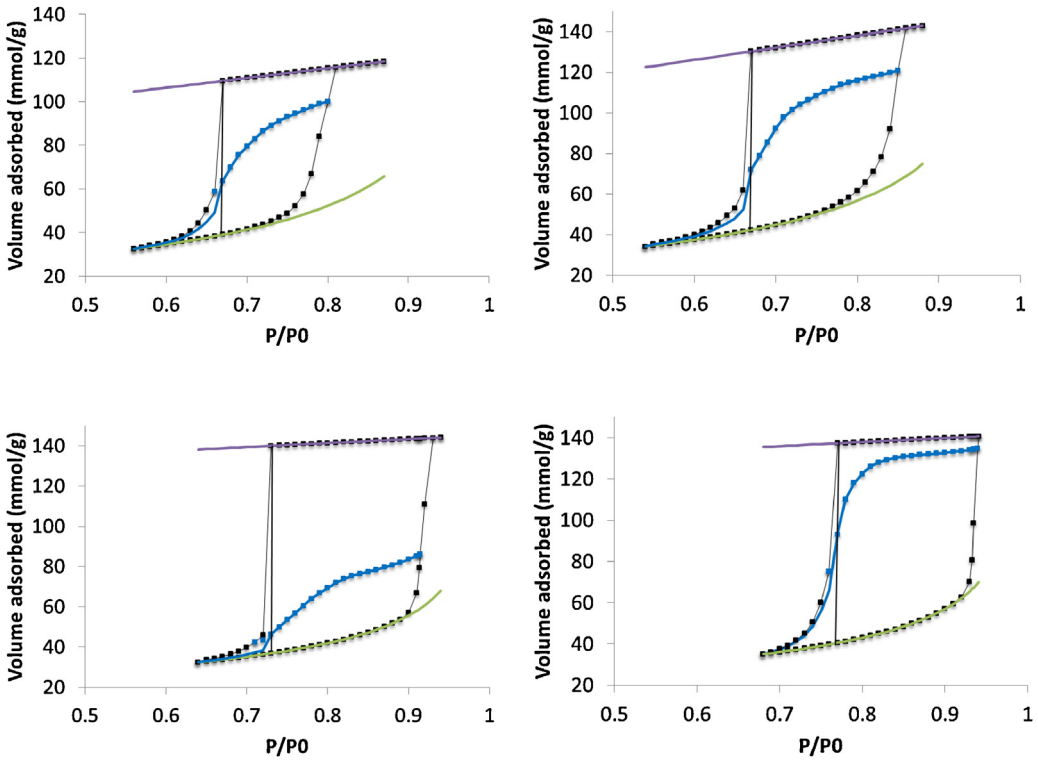

Fig. 12. The main adsorption and desorption isotherms and the scanning isotherm used for determining the network connectivity and neck size distribution calculations of 3DOm carbons. Vertical lines are drawn at $\chi = \chi_E$; intersection with the scanning isotherm represents the point at which Eq. (20) is solved to determine the coordination number. Coordination numbers determined in the Bethe approximation are listed in Table 1. Upper raw: 10 nm, 20 nm, Bottom raw: 30 nm, 40 nm.

fractions of metastable necks q and of initially unfilled pores Q_+. The implemented algorithm draws heavily from the one Newman and Ziff [60] suggested for modeling classical bond or site percolation problems. We considered a 3D cubic lattice of $L \times L \times L$ sites with the outer bonds connected to vapor phase, mimicking the external surface of the porous body. The details of the algorithm can be found in Supporting Information. The calculations were performed for the lattice size $L = 200$. This size was chosen as a compromise between the speed of calculations and the inaccuracy caused by the boundary effects. As shown in Supporting Information, the results with $L = 200$ and $L = 275$ are barely distinguishable, Fig. S2. The simulation results are shown in Fig. 10 (right). The rounding of the percolation probability ($Q_+ = 0$) at the threshold, $q_c \approx 0.25$, is caused by the boundary effects. It is worth noting that the simulation data for the percolation threshold q_c of 3D networks decreases with the coordination number z in accord with the following approximate relationship,

$$q_c \approx \frac{1.5}{z} \tag{19}$$

Although the percolation threshold predicted by the Bethe approximation, Eq. (17), is smaller than that for the real 3D network with same coordination number, the qualitative behavior of the calculated dependencies is quite similar except for the vicinity of the percolation threshold.

5. Use of scanning isotherms for pore structure characterization

Scanning isotherms contain additional information about the specifics of pore structure compared with the primary adsorption and desorption isotherms. As suggested above, PCM may be used to distinguish the materials for which networking effects are present and, as in the example with Vycor glass (Fig. 8, left), to call for the application of percolation models.

5.1. Network connectivity

The network connectivity is characterized by its coordination number z, which determines the percolation threshold q_c according to the Eqs. (17) or (19), depending on the type of the network model. The percolation concept implies that the onset of desorption along the primary desorption isotherm (point E) corresponds to the percolation threshold, however the value of the percolation threshold cannot be determined without additional information. We suggest to determine the coordination number using the scanning desorption isotherm. Indeed, the network connectivity can be estimated from the following relationship for the theoretical fraction of unfilled pores at $\chi = \chi_E$ along the scanning isotherm,

$$Q_-(\chi_E, \chi_a) = Q_+(\chi_a) + (1 - Q_+(\chi_a)) \cdot \alpha(q_c, Q_+(\chi_a)) \tag{20}$$

The fractions of unfilled pores $Q_+(\chi_a)$ and $Q_-(\chi_E, \chi_a)$ are defined from Eqs. (9) and (10), as

$$Q_+(\chi_a) = \frac{V_c(\chi_a) - V_+(\chi_a)}{V_c(\chi_a) - V_s(\chi_a)} \quad \text{and} \quad Q_-(\chi_E, \chi_a) = \frac{V_c(\chi_E) - V_-(\chi_E|\chi_a)}{V_c(\chi_E) - V_s(\chi_E)} \tag{21}$$

Solution of the algebraic equation (20) with respect to q_c for given scanning desorption isotherm $V_-(\chi|\chi_a)$ is straightforward in the Bethe approximation, when the function $\alpha(q_c, Q_+)$ is defined by Eqs. (17) and (18).

Using the Bethe model, we calculated the percolation threshold and the coordination number for the samples of Vycor glass and 3DOm carbons from the scanning isotherms given in Figs. 3 and 4. These data are presented in Table 1.

For Vycor glass, we used two scanning isotherms originating from $\chi_a = 0.34$ and 0.12 to determine the connectivity that produced pretty comparable results. For 3DOm carbons, the scanning isotherm with the largest $Q_+(\chi_a)$ was used for each sample.

Table 1
Coordination number z and percolation threshold q_c determined in the Bethe model from scanning isotherms. The fraction of unfilled pores $Q_+(\chi_a)$ at the onset of scanning at $\chi = \chi_a$ is shown in the 3rd column. For Vycor glass, two scanning isotherms were used to show the difference between the results obtained with different scanning isotherms.

Sample	Vycor	Vycor	3DOm, 10 nm	3DOm, 20 nm	3DOm, 30 nm	3DOm, 40 nm
z	6.6	7.2	6.6	6.6	5.2	5.2
q_c	0.18	0.16	0.18	0.18	0.24	0.24
$Q_+(\chi_A)$	0.34	0.12	0.24	0.27	0.68	0.09

Due to the imprecise definition of the percolation threshold (no sharp knee is present) for these materials, the point E positions were determined by "squaring up" the edges of the primary desorption isotherms. The obtained values of coordination numbers for all the samples are around $z = 6$, which points toward the possibility to employ a simple cubic network as a reasonable 3D model of the pore networks in these samples.

The predictions of the scanning desorption isotherms using the probability factors $\alpha(q, Q_+)$ determined with the chosen value of the coordination number $z = 6.6$ for Vycor glass are presented in Fig. 11. In stark contrast to Fig. 8, the theoretical desorption scanning isotherms agree well with the experimental data with exception of the lowest scanning isotherm, confirming the consistency of the proposed percolation model.

The main adsorption and desorption isotherms together with the scanning isotherm that was used for calculations of connectivity of 3ODm carbons are shown in Fig. 12. The scanning isotherm calculated with the determined coordination number z determined from the experimental value at $\chi = \chi_E$ agrees with the experimental data points in the range: $\chi_E \le \chi < \chi_C$.

5.2. Pore neck size distribution

Once the coordination number of the pore network is determined, one can obtain the dependence of the fraction of metastable necks on the relative pressure, $q(\chi)$, as the following. The fraction of metastable necks at $\chi = \chi_E$ equals the percolation threshold, $q(\chi_E) = q_c$. Above the threshold, for $\chi_A < \chi < \chi_E$, the fraction of metastable necks $q(\chi)$ is determined by the primary desorption isotherm via the percolation probability function $Q_p(q)$ by solving Eq. (16) with respect to q,

$$q(\chi) = Q_p^{-1}\left(\frac{V_c(\chi) - V_-(\chi)}{V_c(\chi) - V_s(\chi)}\right) \quad \text{at} \quad \chi_A < \chi < \chi_E \tag{22}$$

where Q_p^{-1} is the inverse function to $Q_p(q)$, which depends on the coordination number. Below the threshold, for $\chi_E \le \chi < \chi_C$, the fraction of metastable necks $q(\chi)$ is determined from the scanning desorption isotherm via the probability factor $\alpha(q, Q_+(\chi_a))$ by solving Eq. (18) with respect to q.

$$q(\chi) = \alpha^{-1}\left(\frac{Q_-(\chi, \chi_a) - Q_+(\chi_a)}{1 - Q_+(\chi_a)}, Q_+(\chi_a)\right) \quad \text{at} \quad \chi_E \le \chi < \chi_C \tag{23}$$

where α^{-1} is the inverse function to $\alpha(q, Q_+(\chi_a))$, the fraction of unfilled pores $Q_+(\chi_a)$ and $Q_-(\chi, \chi_a)$ are defined respectively by (6) and from (10), as

$$Q_-(\chi, \chi_a) = \frac{V_c(\chi) - V_-(\chi, \chi_a)}{V_c(\chi) - V_s(\chi)} \tag{24}$$

The fraction of the metastable necks as a function of the relative pressure, $q(\chi)$, determined according to the above scheme for Vycor glass is presented in Fig. 13 for two percolation models, the Bethe approximation on the left panel, and 3D cubic lattice simulation on the right panel. It the former case, the two parts of the $q(\chi)$ function determined from the main desorption isotherm at $\chi_A < \chi < \chi_E$ and from the scanning isotherm at $\chi_E \le \chi < \chi_C$ merge at $\chi = \chi_E$, since the condition $q(\chi_E) = q_c$ is fulfilled for both Eqs. (22) and (23) due to the choice of the coordination number z from Eq. (19). For the cubic lattice model with the predetermined coordination number z = 6 and percolation threshold of 0.25, there is a step at $\chi = \chi_E$, due to a mismatch of data derived from the main and the scanning isotherms. However, this step is minor, and it does not affect the neck size distribution derived from the $q(\chi)$ function significantly, as shown below (Fig. 15). The same approach for determining the fractions of metastable necks $q(\chi)$ was applied for 3DOm carbons (Fig. 14). The isotherms used for calculations are shown in Fig. 12. The calculated PSDs are presented in Fig. 16 in the same style used for Vycor glass in Fig. 15. In all cases, the difference between the results obtained from the Bethe approximation and from the 3D cubic lattice simulation is insignificant for practical applications.

The pore neck distribution is obtained by using a certain correlation between the neck size d_n and the relative pressure $\chi_-(d_n)$, at which fluid in this pore becomes metastable. The function

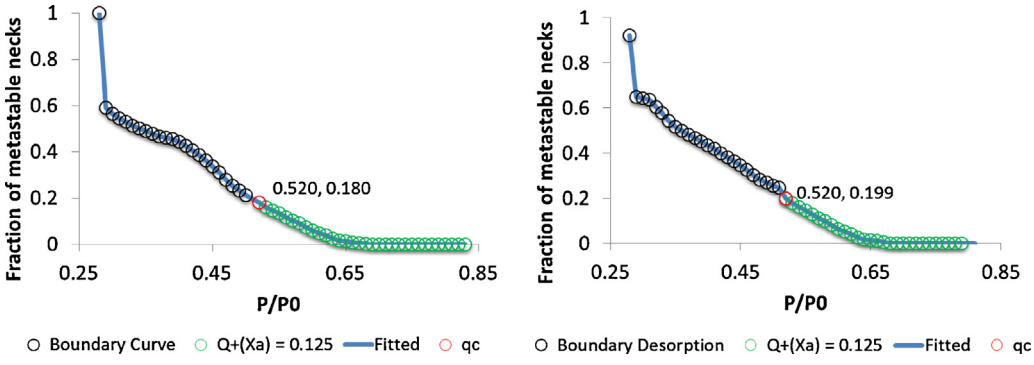

Fig. 13. The fraction of the metastable necks as a function of the relative pressure, $q(\chi)$, for Vycor glass [1], calculated using the scanning isotherm with $Q_+(\chi_a) = 0.125$. Bethe approximation (left) and 3D cubic lattice MC simulation (right).

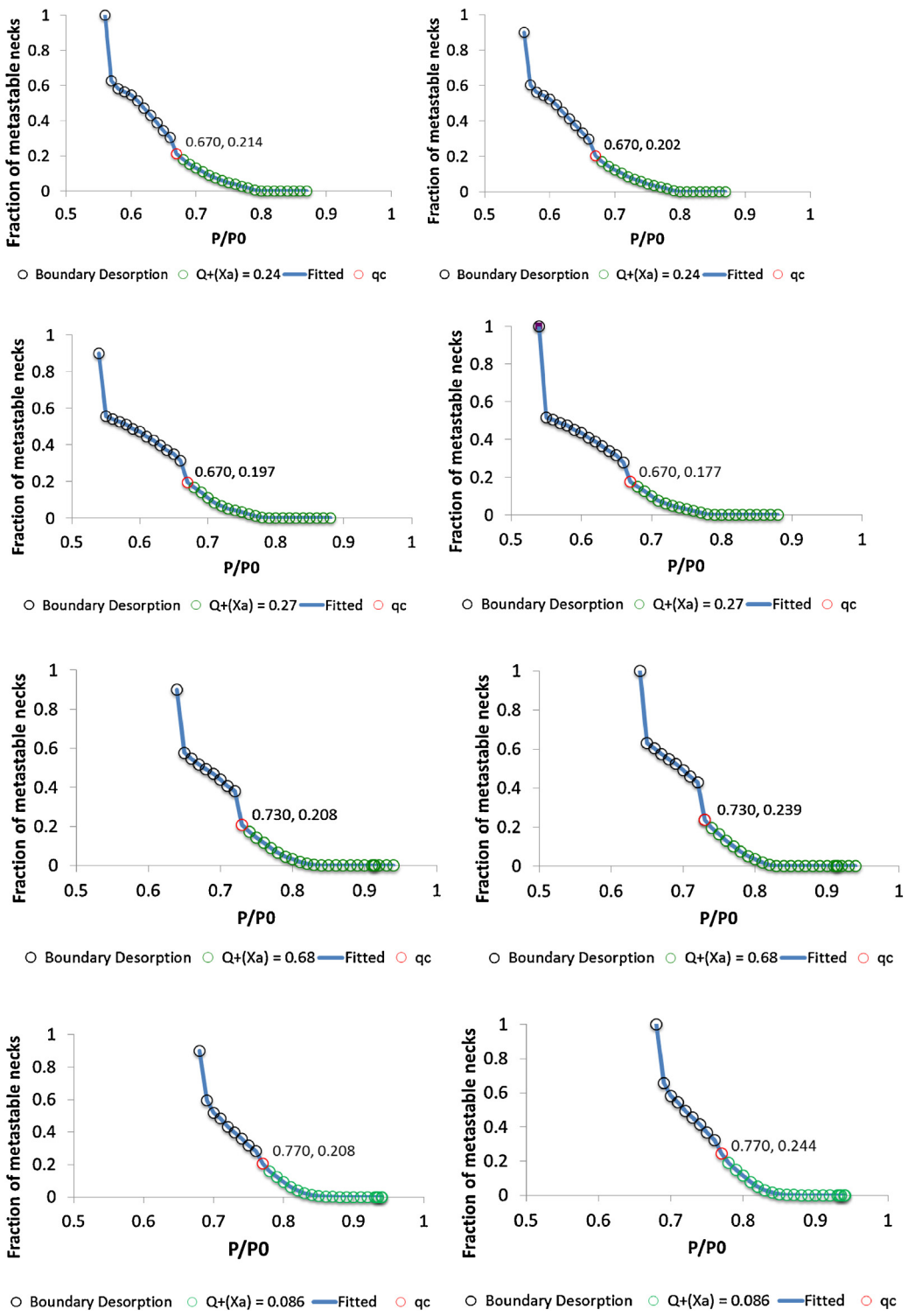

Fig. 14. The fraction of the metastable necks, $q(\chi)$, as a function of the relative pressure for 3DOm Carbons. using the 3D cubic lattice MC simulation (left) and Bethe approximation with fitted coordination number (right). From top to bottom: 10 nm, $Q_+(\chi_a) = 0.24$; 20 nm, $Q_+(\chi_a) = 0.27$; 30 nm, $Q_+(\chi_a) = 0.68$; 40 nm, $Q_+(\chi_a) = 0.09$.

$q(\chi)$ determines the integral number distribution function, $\phi_n(d_n)$, which represents the fraction of necks smaller than d_n, as

$$\phi_n(d_n) = 1 - q(\chi_-(d_n)) \tag{25}$$

Let us introduce another distribution function, which has a more direct relevance to the evaporation process. Indeed, the condition of evaporation from an individual pore is mainly determined by the size of the largest neck. As such, the probability, $\phi_m(d_n)$, that the largest neck is smaller than d_n, and the number distribution, $\phi_n(d_n)$, are related via the balance of probabilities,

$$\phi_m(d_n) = (\phi_n(d_n))^z \tag{26}$$

The second term in the RHS of Eq. (26) equals the probability that all z necks of the pore are smaller than d_n.

The neck size distributions $\phi_n(d_n)$ and the pore distribution by the largest neck, $\phi_m(d_n)$ complement the pore size distribution,

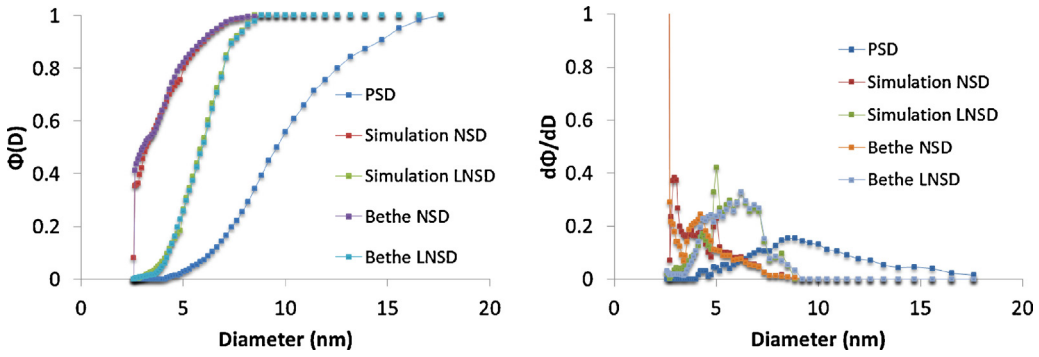

Fig. 15. Integral (left) and differential (right) distributions for Vycor [1]. Pore size distribution (PSD), $\phi_p(d_p)$, calculated from Eq. (27) (blue curves). Neck size distribution (NSD), $\phi_n(d_n)$, and largest neck size distribution (LNSD), $\phi_m(d_n)$, were calculated using the Bethe model, (purple curves) and using the 3D cubic lattice simulation (red curves). Note the striking similarity in the neck size distributions obtained with the two methods. (For interpretation of the references to color in this sentence, the reader is referred to the web version of the article.)

$\phi_p(d_p)$. The latter is determined from the main adsorption isotherm, assuming that the fraction of unfilled pores $Q_+(\chi)$ gives the fraction of pores larger than d_p, condensation in which does not occur at the relative pressure $\chi = \chi_+(d_p)$,

$$\phi_p(d_p) = 1 - Q_+(\chi_+(d_p)) \tag{27}$$

Note that thus defined $\phi_p(d_p)$ is the integral number distribution function.

The integral and differential distribution functions for pore and neck diameters for Vycor glass are presented in Fig. 15. In this case, we used the Kelvin equation for Xenon at 225 K to correlate the pore and neck size and the relative pressures of condensation and desorption, $\chi_+(d_p)$ and $\chi_-(d_n)$. Although the Kelvin equation underestimates the pore size at the nanoscale [61] this choice is dictated by unavailability of more advanced methods for Xe adsorption.

For calculations of PSDs in 3DOm carbons, we used the QSDFT relationships for spherical (pore) and cylindrical (neck) pore geometries for argon on carbon derived in Ref.[40] to correlate the pore and neck size and the relative pressures of condensation and desorption, $\chi_+(d_p)$ and $\chi_-(d_n)$. The neck side distributions were calculated using the proposed percolation models, the Bethe approximation and the 3D cubic lattice MC simulation. The pore size distribution was calculated from the adsorption isotherm by the QSDFT method [40], rather than via Eq. (27). The results of thus calculated differential pore and neck size distributions are presented in Fig. 16; the same style and denotations are used as in Fig. 15 (right).

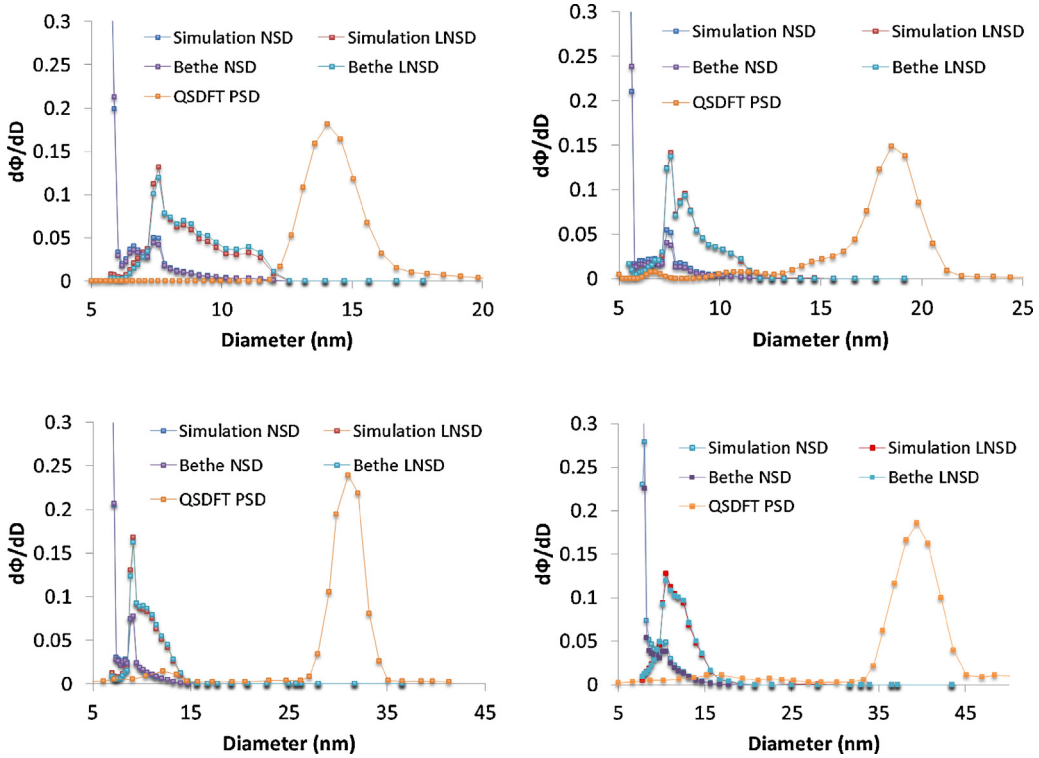

Fig. 16. Differential PSDs for 3DOm carbons; (top left to bottom right) 10 nm, 20 nm, 30 nm, and 40 nm carbons. Pore size distribution (PSD), $\phi_p(d_p)$ (orange curves), calculated by the QSDFT method from the main adsorption isotherm [40]. Neck size distribution (NSD), $\phi_n(d_n)$, and largest neck size distribution (LNSD), $\phi_m(d_n)$, were calculated from the main and scanning desorption isotherms shown in Fig. 14 using the percolation method; the Bethe model (purple curves) and the 3D cubic lattice MC simulation (red curves). Note the striking similarity in the neck size distributions obtained with the two methods for all the samples. (For interpretation of the references to color in this sentence, the reader is referred to the web version of the article.)

Please cite this article in press as: R. Cimino, et al., Experimental and theoretical studies of scanning adsorption–desorption isotherms, Colloids Surf. A: Physicochem. Eng. Aspects (2013), http://dx.doi.org/10.1016/j.colsurfa.2013.03.025

Two conclusions can be drawn from Figs. 15 and 16. First, the neck size distributions, $\phi_n(d_n)$, and largest neck size distributions, $\phi_m(d_n)$, calculated using the Bethe model and the 3D cubic lattice simulation are very similar, almost indistinguishable for any practical application. As such, one can use the Bethe approximation for practical calculations of the network connectivity and the neck size distribution using experimental data on the main and scanning desorption isotherms. Secondly, the distribution of the pores by the largest neck size better reflects the structural features of pore networks than the distribution of neck sizes, and can be recommended as a complement to the pore size distribution to be used in establishing the structure–property relations.

6. Summary

Although the phenomenon of adsorption hysteresis has been attracting a lot of attention among both experimental and theoretical communities for several generations of researchers, its adequate description, despite major progress achieved in recent years, is still lacking for complex porous systems. Indeed, the interplay between the thermodynamic and geometrical factors gives rise to distinct features of hysteresis in different materials. Experimentally, these distinct features are prominently displayed in the behavior of scanning isotherms, which provide additional information about the pore network geometry, including its connectivity and pore size distribution, which cannot be revealed from the main adsorption and desorption branches. Theoretically, it has been well understood since the seminal works of Everett [1] that the description of scanning isotherms cannot be achieved based on the models of adsorption in individual pores; it is necessary to take into account a cooperative nature of capillary condensation and desorption processes in three dimensional pore networks with distributed geometrical parameters of individual pores.

In this work, we analyze adsorption and desorption scanning isotherms on porous materials of different yet well characterized structure: regular hexagonal array of pore channels in SBA-15 silica, cubically ordered three dimensional gyroid structure in KIT-6 silica, ordered three dimensional network of spheroidal cages in 3DOm carbons. The classical system of Xenon adsorption on disordered pore network of Vycor porous glass [16] is served as a reference system.

Firstly, we analyze the limitations of the models of individual pores and suggest an original partial correlation model (PCM) to distinguish the importance of the pore blocking effects. We show that while PCM satisfactorily describes the behavior of scanning isotherms on SBA-15 silica with independent pore channels, the deviation between the experimental and theoretical scanning desorption isotherms found for other samples and especially for Vycor glass point toward the necessity to account for the pore blocking effects. As such, PCM applied to scanning desorption isotherms is suggested as a test for the pore blocking effects.

Secondly, we revisit and advance the percolation model of adsorption hysteresis put forward earlier by one of us [24] for simulating the scanning desorption process in the pore and neck networks. Two percolation models were implemented: an analytical Bethe approximation and a Monte Carlo simulation on the 3D cubic lattice. We show that both models reasonably describe the behavior of scanning desorption isotherms. We formulate a method for determining the effective pore network coordination number z from the consistency condition of the Bethe approximation applied to the main desorption and scanning desorption isotherms. The network coordination number characterizes the connectivity of the pore structure. Interestingly, the coordination numbers for Vycor glass and four different samples of 3DOm carbons were found in the range between 5 and 7 that justifies the use of the 3D cubic lattice with $z = 6$ as a structural model of pore structures in these materials.

Thirdly, we suggest a percolation method for calculating the distributions of pore neck sizes using experimental data on the main adsorption and desorption isotherms and one scanning desorption isotherm. The proposed method is illustrated on the Vycor glass and 3DOm samples.

As such, we attempted to lay groundwork for developing a practical methodology for calculating the network connectivity and pore size distributions from the scanning isotherms. With the current accuracy of high-resolution adsorption measurements, which provides an opportunity of measuring scanning isotherms in automated regimes of commercial instruments, this desired methodology becomes feasible. It may provide new useful information about the geometrical specifics of pore networks in novel designer nanomaterials.

Acknowledgments

AVN gratefully acknowledges support from the Rutgers NSF ERC on Structural Organic Particulate Systems. RTC thanks Dr. Mark Newman for useful discussions of percolation theory simulation. M.T. thanks Prof. Freddy Kleitz for providing SBA-15 and KIT-6 samples for adsorption studies.

Appendix A. Supplementary data

Supplementary data associated with this article can be found, in the online version, at http://dx.doi.org/10.1016/j.colsurfa.2013.03.025.

References

[1] D.H. Everett, Adsorption hysteresis, in: E.A. Flood (Ed.), The Solid–Gas Interface, Decker, New York, 1967, pp. 1055–1113.
[2] J. Roquerol, F. Roquerol, K.S.W. Sing, Adsorption by Powders and Porous Solids: Principles, Methodology and Applications, Academic Press, London, UK, 1998.
[3] T. Horikawa, D.D. Do, D. Nicholson, Capillary condensation of adsorbates in porous materials, Adv. Colloid Interface Sci. 169 (2011) 40–58.
[4] P.A. Monson, Understanding adsorption/desorption hysteresis for fluids in mesoporous materials using simple molecular models and classical density functional theory, Microporous Mesoporous Mater. 160 (2012) 47–66.
[5] J. Rouquerol, D. Avnir, C.W. Fairbridge, D.H. Everett, J.M. Haynes, N. Pernicone, J.D.F. Ramsay, K.S.W. Sing, K.K. Unger, Recommendations for the characterization of porous solids, IUPAC Recomm. 66 (1994) 1739–1758.
[6] J.S.S. Lowell, J.E. Shields, M.A. Thomas, M. Thommes, Surface Area, Porosity and Density, Kluwer Academic Publishers, The Netherlands, 2004.
[7] R. Zsigmondy, Über die Struktur des Gels der Kieselsäure. Theorie der Entwässerung, Z. Anorg. Allgem. Chemie 71 (1911) 356–377.
[8] E.O. Kraemer, Treatise on Physical Chemistry, Van Nostrand, New York, 1931.
[9] J.W. McBain, An explanation of hysteresis in the hydration and dehydration of gels, J. Am. Chem. Soc. 57 (1935) 699–700.
[10] L.H. Cohan, Sorption hysteresis and the vapor pressure of concave surfaces, J. Am. Chem. Soc. 60 (1938) 433–435.
[11] L.H. Cohan, Hysteresis and the capillary theory of adsorption of vapors, J. Am. Chem. Soc. 66 (1944) 98–105.
[12] R.K. Schofield, General discussion, Faraday Discuss. 3 (1948) 105.
[13] J.H. DeBoer, Structure and Properties of Porous Materials, Colston Papers, vol. 10, 195868.
[14] M.M. Dubinin, B.P. Bering, V.V. Serpinsky, B.N. Vasilev, in: J.F. Danielli, K.G.A. Pankhurst, A.C. Riddiford (Eds.), Surface Phenomena in Chemistry and Biology, Pergamon, New York, 1958, p. 172.
[15] J.M. van Bemmelen, Die Absorption das Wasser in den Kolloiden, besonders in dem Gel der Kieselsäure, Z. Anorg. Allg. Chem. 13 (1897) 233–356.
[16] A.J. Brown, Ph.D. Thesis (1963) 14–107.
[17] A.V. Neimark, Percolation theory of capillary hysteresis phenomena and its applications for characterization of porous solids, Stud. Surf. Sci. Catal. 62 (1991) 67–74.
[18] G.C. Wall, R.J.C. Brown, The determination of pore-size distributions from sorption isotherms and mercury penetration in interconnected pores: the application of percolation theory, J. Colloid Interface Sci. 82 (1981) 141–149.
[19] A.V. Neimark, Theory of capillary phenomena in porous-media and its application, Khimicheskaya Promyshlennost (Sov. Chem. Ind.) (11) (1981) 656–659.
[20] A.V. Neimark, Development of theory of capillary condensation and desorption in mesopores of adsorbents, on the basis of lattice models of pore structure, Dokl. Akad. Nauk SSSR (REP ACAD SCI USSR) 273 (1983) 384–388.

[21] L.I. Kheifets, A.V. Neimark, Multiphase Processes in Porous Media, Khimia, Moscow, 1982.
[22] G. Mason, The effect of pore space connectivity on the hysteresis of capillary condensation in adsorption–desorption isotherms, J. Colloid Interface Sci. 88 (1982) 36–46.
[23] G. Mason, A model of adsorption–desorption hysteresis in which hysteresis is primarily developed by the interconnections in a network of pores, Proc. R. Soc. Lond. A: Math. Phys. Sci. 390 (1983) 47–72.
[24] A.V. Neimark, Theory of the calculation of scanning adsorption and desorption isotherms in mesophorous adsorbents, Colloid J. USSR 46 (1984) 1004–1010.
[25] G. Mason, Determination of the pore-size distributions and pore-space interconnectivity of Vycor porous glass from adsorption desorption hysteresis capillary condensation isotherms, Proc. R. Soc. Lond. A: Math. Phys. Sci. 415 (1988) 453–486.
[26] M. Parlar, Y.C. Yortsos, Percolation theory of vapor adsorption desorption processes in porous materials, J. Colloid Interface Sci. 124 (1988) 162–176.
[27] M. Parlar, Y.C. Yortsos, Nucleation and pore geometry effects on capillary desorption in porous media, J. Colloid Interface Sci. 132 (1989) 425–443.
[28] D. Wilkinson, J.F. Willemsen, Invasion percolation: a new form of percolation theory, J. Phys. A 16 (1983) 3365–3376.
[29] A.V. Neimark, Application of lattice models of porous structure for investigation of mercury porosimetry, Colloid J. USSR 46 (1984) 727–734.
[30] A.V. Neimark, Application of lattice models of adsorbents and catalysts in studies of their capillary properties. Analysis of scanning curves for mercury intrusion and extraction, Colloid J. USSR 47 (1985) 86–92.
[31] N.A. Seaton, Determination of the connectivity of porous solids from nitrogen sorption measurements, Chem. Eng. Sci. 46 (1991) 1895–1909.
[32] H.L. Liu, L. Zhang, N.A. Seaton, Analysis of sorption hysteresis in mesoporous solids using a pore network model, J. Colloid Interface Sci. 156 (1993) 285–293.
[33] M.P. Lilly, P.T. Finley, R.B. Hallock, Memory, congruence and avalanche events in hysteretic capillary condensation, Phys. Rev. Lett. 71 (1993) 4186–4189.
[34] P. Rajniak, R.T. Yang, A simple-model and experiments for adsorption–desorption hysteresis – water–vapor on silica-gel, AIChE J. 39 (1993) 774–786.
[35] P. Rajniak, R.T. Yang, Hysteresis-dependent adsorption–desorption cycles – generalization for isothermal conditions, AIChE J. 40 (1994) 913–924.
[36] V. Mayagoitia, F. Rojas, I. Kornhauser, Pore network interactions in ascending processes relative to capillary condensation, J. Chem. Soc. Faraday Trans. I 81 (1985) 2931–2940.
[37] S. Cordero, F. Rojas, I. Kornhauser, A. Dominguez, A. Vidales, R. Lopez, G. Zgrablich, J.L. Riccardo, Pore-blocking and pore-assisting factors during capillary condensation and evaporation, Appl. Surf. Sci. 196 (2002) 224–238.
[38] F. Rojas, I. Kornhauser, C. Felipe, J.M. Esparza, S. Cordero, A. Dominguez, J.L. Riccardo, Capillary condensation in heterogeneous mesoporous networks consisting of variable connectivity and pore-size correlation, Phys. Chem. Chem. Phys. 4 (2002) 2346–2355.
[39] A.V. Neimark, Percolation method of calculation of pore dimension distribution in mesoporous materials based on adsorption and desorption isotherms in the hysteresis loop, Zh. Fiz. Khim. 60 (1986) 1745–1750.
[40] K.A. Cychosz, X. Guo, W. Fan, R. Cimino, G.Y. Gor, M. Tsapatsis, A.V. Neimark, M. Thommes, Characterization of the pore structure of three-dimensionally ordered mesoporous carbons using high resolution gas sorption, Langmuir 28 (2012) 12647–12654.
[41] N.K. Kanellopoulos, Nanoporous Materials: Advanced Techniques for Characterization, Modeling and Processing, CRC Press Taylor & Francis Distributor, Boca Raton, FL, 2011.
[42] G.Q. Lu, X.S. Zhao, Nanoporous Materials: Science Engineering, Imperial College Press, London, 2004.
[43] J. Tascon, Novel Carbon Adsorbents, 1st ed., Elsevier, Oxford, UK, 2012.
[44] D.Y. Zhao, J.L. Feng, Q.S. Huo, N. Melosh, G.H. Fredrickson, B.F. Chmelka, G.D. Stucky, Triblock copolymer syntheses of mesoporous silica with periodic 50 to 300 angstrom pores, Science 279 (1998) 548–552.
[45] G.A. Tompsett, L. Krogh, D.W. Griffin, W.C. Conner, Hysteresis and scanning behavior of mesoporous molecular sieves, Langmuir 21 (2005) 8214–8225.
[46] A. Grosman, C. Ortega, Nature of capillary condensation and evaporation processes in ordered porous materials, Langmuir 21 (2005) 10515–10521.
[47] T.W. Kim, F. Kleitz, B. Paul, R. Ryoo, MCM-48-like large mesoporous silicas with tailored pore structure: Facile synthesis domain in a ternary triblock copolymer–butanol–water system, J. Am. Chem. Soc. 127 (2005) 7601–7610.
[48] F. Kleitz, T.W. Kim, R. Ryoo, Design of mesoporous silica at low acid concentrations in triblock copolymer–butanol–water systems, Bull. Korean Chem. Soc. 26 (2005) 1653–1668.
[49] F. Kleitz, F. Berube, R. Guillet-Nicolas, C.-M. Yang, M. Thommes, Probing adsorption, pore condensation, and hysteresis behavior of pure fluids in three-dimensional cubic mesoporous KIT-6 silica, J. Phys. Chem. C 114 (2010) 9344–9355.
[50] W. Fan, M.A. Snyder, S. Kumar, P.-S. Lee, W.C. Yoo, A.V. McCormick, R.L. Penn, A. Stein, M. Tsapatsis, Hierarchical nanofabrication of microporous crystals with ordered mesoporosity, Nat. Mater. 7 (2008) 984–991.
[51] T.H. Elmer, Porous and reconstructed glasses, in: S.J. Schneider (Ed.), Engineered Materials Handbook, ASM International, Materials Park, OH, 1990, pp. 427–432.
[52] L.D. Gelb, K.E. Gubbins, Characterization of porous glasses: simulation models, adsorption isotherms, and the Brunauer–Emmett–Teller analysis method, Langmuir 14 (1998) 2097–2111.
[53] E. Kierlik, M. Rosinberg, J.E. Finn, P.A. Monson, Binary vapor mixtures adsorbed on a graphite surface – a comparison of mean field density functional theory with results from Monte-carlo simulations, Mol. Phys. 75 (1992) 1435–1454.
[54] D.H. Everett, A general approach to hysteresis. Part 3. A formal treatment of the independent domain model of hysteresis, Trans. Faraday Soc. 50 (1954) 1077–1096.
[55] D.H. Everett, F.W. Smith, A general approach to hysteresis. Part 2. Development of the domain theory, Trans. Faraday Soc. 50 (1954) 187–197.
[56] P. Ravikovitch, A.V. Neimark, Characterization of micro- and mesoporosity in SBA-15 materials from adsorption data by the NLDFT method, J. Phys. Chem. B 105 (2001) 6817–6823.
[57] M. Thommes, B. Smarsly, M. Groenewolt, P.I. Ravikovitch, A.V. Neimark, Adsorption hysteresis of nitrogen and argon in pore networks and characterization of novel micro- and mesoporous silicas, Langmuir 22 (2006) 756–764.
[58] C. Rasmussen, A. Vishnyakov, M. Thommes, B. Smarsly, F. Kleitz, A.V. Neimark, Cavitation in metastable liquid nitrogen confined to nanoscale pores, Langmuir 26 (2010) 10147–10157.
[59] M. Sahimi, Applications of Percolation Theory, Taylor & Francis, London, 1994.
[60] M.E.J. Newman, R.M. Ziff, Fast Monte Carlo algorithm for site or bond percolation, Phys. Rev. E 64 (2001) 1–12.
[61] A.V. Neimark, P.I. Ravikovitch, Capillary condensation in mesoporous molecular sieves and pore structure characterization, Microporous Mesoporous Mater. 44–45 (2001) 697–707.

Please cite this article in press as: R. Cimino, et al., Experimental and theoretical studies of scanning adsorption–desorption isotherms, Colloids Surf. A: Physicochem. Eng. Aspects (2013), http://dx.doi.org/10.1016/j.colsurfa.2013.03.025